science.sciencemag.org/cgi/content/full/science.abb3405/DC1

Supplementary Materials for

Crystal structure of SARS-CoV-2 main protease provides a basis for design of improved α-ketoamide inhibitors

Linlin Zhang, Daizong Lin, Xinyuanyuan Sun, Ute Curth, Christian Drosten, Lucie Sauerhering, Stephan Becker, Katharina Rox, Rolf Hilgenfeld*

*Corresponding author. Email: rolf.hilgenfeld@uni-luebeck.de

Published 20 March 2020 on *Science* First Release
DOI: 10.1126/science.abb3405

This PDF file includes:

Materials & Methods

Recombinant protein production

A gene encoding SARS-CoV-2 M^{pro} (ORF1ab polyprotein residues 3264-3569, GenBank code: MN908947.3) with *Escherichia coli (E. coli)* codon usage was synthesized by MWG Eurofins. The synthesized gene was first amplified with the forward primer 5′-TCGGGGTTTCGCAAAAT-3′ and the reverse primer 5′-CTGAAACGTGACACCGCTACA-3′. Subsequently, this PCR product was employed as the template for the amplification of the target gene with primers (forward) 5′-CGCGGATCCTCGGCAGTGCTGCAATCGGGGTTTCGCAAAAT-3′, and (reverse) 5′-CCGCTCGAGTTAATGATGATGATGATGATGGGGTCCCTGAAACGTGACACCGCTACAC T -3′ including the cleavage sites of restriction enzymes for cloning into the vector PGEX-6p-1 (GE Healthcare). The amplified PCR product was digested with *BamHI* and *XhoI* and ligated into the vector PGEX-6p-1 digested with the same restriction enzymes. At the N-terminus, the construct designed for SARS-CoV-2 M^{pro} contains the M^{pro} cleavage-site (SAVLQ↓SGFRK; arrow indicates the cleavage site) corresponding to the cleavage site between Nsp4 and Nsp5 in the polyprotein of this virus. At the C-terminus, the construct codes for a modified PreScission cleavage site (SGVTFQ↓GP; the six-residue sequence at the C-terminus of the SARS-CoV-2 M^{pro} was used as P6-P1 for PreScission cleavage) connected to a His_6-tag. An authentic N-terminus was generated during gene expression by auto-cleavage of the M^{pro} itself, and the authentic C-terminus was generated after the treatment with PreScission protease, similar to the approach described for SARS-CoV M^{pro} in *(20)*. The gene sequence of the M^{pro} was verified by sequencing at MWG Eurofins.

The sequence-verified SARS-CoV-2 M^{pro} construct was transformed into *E. coli* strain BL21-Gold (DE3) (Novagen). Transformed clones were pre-cultured at 37°C in 50 mL 1 x YT

medium with ampicillin (100 μg/mL) for 3 h, and the incubated culture was inoculated into 4 L 1 x YT medium supplied with 100 μg/mL ampicillin. 0.5 mM isopropyl-D-thiogalactoside (IPTG) was added for induction of the overexpression of the M^{pro} gene at 37°C when the OD_{600} reached 0.8. After 5 h, cells were harvested by centrifugation at 9954 x *g*, 4°C for 15 min. The pellets were resuspended in 30 mL buffer A (20 mM Tris, 150 mM NaCl, pH 7.8; pH of all buffers was adjusted at room temperature) and then lysed by sonication on ice. The lysate was clarified by ultracentrifugation at 146,682 x *g* at 4°C for 1 h. The supernatant was loaded onto a HisTrap FF column (GE Healthcare) equilibrated with buffer A. The HisTrap FF column was washed with 150 mL buffer A to remove unspecific binding proteins, followed by elution using buffer B (20 mM Tris, 150 mM NaCl, 500 mM imidazole, pH 7.8) with a linear gradient of imidazole ranging from 0 mM to 500 mM, 20 column volumes. The fractions containing target protein were pooled and mixed with PreScission protease at a molar ratio of 5:1 and dialyzed into buffer C (20 mM Tris, 150 mM NaCl, 1 mM DTT, pH 7.8) at 4°C overnight, resulting in the target protein with authentic N- and C-termini. The PreScission-treated M^{pro} was applied to connected GSTtrap FF (GE Healthcare) and nickel columns to remove the GST-tagged PreScission protease, the His-tag, and protein with uncleaved His-tag. The His-tag-free M^{pro} in the flow-through was subjected to buffer exchange with buffer D (20 mM Tris, 1 mM DTT, pH 8.0) by using Amicon Ultra 15 centrifugal filters (10 kD, Merck Millipore) at 2773 x *g*, and 4°C. The protein was loaded onto a HiTrap Q FF column (GE Healthcare) equilibrated with buffer D for further purification. The column was eluted by buffer E (20 mM Tris, 1 M NaCl, 1 mM DTT, pH 8.0) with a linear gradient ranging from 0 to 500 mM NaCl (20 column volumes buffer). Fractions eluted from the Hitrap Q FF column containing the target protein with high purity were pooled and subjected to buffer exchange (20 mM Tris, 150 mM NaCl, 1 mM EDTA, 1 mM DTT, pH 7.8).

Cloning, gene expression, and protein purification of SARS-CoV M^{pro} was performed according to *(20)* and *(14)*.

Crystallization of the free SARS-CoV-2 M^{pro}

A freshly prepared protein solution at a concentration of 25 mg/mL was cleared by centrifugation at 12,000 x *g*. Subsequently, a basic screen with the commercially available screening kit PACT premier™ HT-96 (Molecular Dimensions) was performed by using a Gryphon LCP crystallization robot (Art Robbins) employing the sitting-drop vapor-diffusion method at 18°C. 0.15 µL of protein solution and 0.15 µL of reservoir were mixed to equilibrate against 40 µL reservoir solution. Crystals appeared overnight under several conditions, e.g. condition B5 (0.1 M MIB (sodium malonate, imidazole, and boric acid in molar ratio 2:3:3), pH 8.0, 25% polyethylene glycol (PEG) 1,500), condition D4 (0.1 M MMT (DL-malic acid, MES, and Tris base in molar ratio 1:2:2), pH 7.0, 25% PEG 1,500), condition E9 (0.2 M potassium sodium tartrate tetrahydrate, 20% PEG 3,350), etc. Crystals were fished from the drops and cryo-protected by mother liquor plus varied concentrations of glycerol (10%-20%). Subsequently, fished crystals were flash-cooled in liquid nitrogen.

Crystallization of 13b in complex with SARS-CoV-2 M^{pro}

Freshly prepared protein (as described above) at a concentration of 25 mg/mL was mixed with **13b** (dissolved in 100% DMSO) at a molar ratio of 1:5. The mixture was incubated at 4°C overnight. The next day, centrifugation was applied (12,000 x *g*) to remove the white precipitate. Subsequently, the supernatant was subjected to crystallization screening using the same method as

described above for the crystallization of the free enzyme. A basic screen was applied by using three commercially available kits: PEGRx™ 1 & 2 (Hampton Research), PACT premier™ HT-96 (Molecular Dimensions), and Morpheus HT-96 (Molecular Dimensions). Crystals appeared overnight under conditions No. 45 (0.1 M bicine, pH 8.5, 20% PEG 10,000) of PEGRx™ 1 and No. 39 (10% PEG 200, 0.1 M bis-tris propane, pH 9.0, 18% PEG 8,000) of PEGRx™ 2, condition G9 (0.1 M Carboxylic acids (0.2 M sodium formate, 0.2 M ammonium acetate, 0.2 M sodium citrate tribasic dihydrate, 0.2 M potassium sodium tartrate tetrahydrate, 0.2 M sodium oxamate), 0.1 M buffer system 3 (1.0 M Tris, bicine, pH 8.5), pH 8.5, 30% precipitant mix 1 (20% v/v PEG 500 methyl ether, 10% PEG 20,000)) of Morpheus HT-96. Manual reproduction was performed by mixing 0.5 µL of complex and 0.5 µL of reservoir, equilibrating against 40 µL of reservoir in a 96-well plate under condition No. 45 of PEGRx™ 1 and No. 39 of PEGRx™ 2, No. G9 of Morpheus HT-96, by using the sitting-drop vapor-diffusion method. Crystals appeared also overnight in the manually reproduced drops. Crystals were fished from the reproduced condition-45 drop (cryo-protectant: mother liquor plus 15% glycerol, and 5 mM **13b**), the reproduced condition-39 drop (cryo-protectant: mother liquor plus 5 mM **13b**), and the original condition-G9 drop (cryo-protectant: mother liquor plus 5 mM **13b**). Subsequently, fished crystals were flash-cooled in liquid nitrogen.

Diffraction data collection, phase determination, model building, and refinement

All diffraction data sets were collected using synchrotron radiation of wavelength 0.9184 Å at beamline BL14.2 of BESSY (Berlin, Germany), using a Pilatus3S 2M detector (Dectris) *(21)*. The data set of the free SARS-CoV-2 M^{pro} was collected from a crystal grown under condition No. D4 of the PACT premier™ HT-96 in the basic screen 96-well plate. Two data sets of the SARS-CoV-2

M^{pro} in complex with **13b** were collected from the crystals grown under condition No. 39 of PEGRx™ 2 (manual optimization) and No. G9 of Morpheus HT-96, respectively. *XDSapp (22)*, *Pointless (23, 24)*, and *Scala (23)* (the latter two from the CCP4 suite *(25)*) were used for processing the datasets. The diffraction dataset of the free SARS-CoV-2 M^{pro} was processed at a resolution of 1.75 Å, in space group *C*2 (Table S2). For the complex of SARS-CoV-2 M^{pro} with **13b**, the dataset collected from a condition-39 crystal was processed at a resolution of 1.95 Å and in space group *C*2 (Table S2), whereas the dataset collected from a condition-G9 crystal extended to a Bragg spacing of 2.20 Å, in space group $P2_12_12_1$ (Table S2). All three structures were determined by molecular replacement with the crystal structure of the free enzyme of the SARS-CoV M^{pro} (PDB entry 2BX4 *(7)*) as search model, using the *Molrep* program *(25, 26)*. *Jligand* from the CCP4 suite *(25, 27)* was employed for the generation of the geometric restraints for **13b**, and the inhibitor was built into the F_o-F_c density by using the *Coot* software *(28)*. Refinement of the three structures was performed with *Refmac5 (25, 29)*. Statistics of diffraction data processing and the model refinement are given in Table S2.

Enzyme kinetics of SARS-CoV-2 and SARS-CoV M^{pro}

A fluorescent substrate harboring the cleavage site (indicated by the arrow, ↓) of SARS-CoV-2 M^{pro} (Dabcyl-KTSAVLQ↓SGFRKM-E(Edans)-NH_2; GL Biochem) and buffer composed of 20 mM Tris, 100 mM NaCl, 1 mM EDTA, 1 mM DTT, pH 7.3 was used for the inhibition assay. In the fluorescence resonance energy transfer (FRET)-based cleavage assay *(14)*, the fluorescence signal of the Edans generated due to the cleavage of the substrate by the M^{pro} was monitored at an emission wavelength of 460 nm with excitation at 360 nm, using a Flx800 fluorescence spectrophotometer (BioTek). Initially, 2.5 μL of the SARS-CoV-2 or SARS-CoV M^{pro} at the final

concentration of 2.0 μM was pipetted into a 96-well plate containing pre-pipetted 22.5 μL reaction buffer. Afterwards, the reaction was initiated by addition of 25 μL of the substrate dissolved in the reaction buffer to 50 μL final volume, at different final concentrations varied from 5 to 640 μM (5, 10, 20, 40, 80, 160, 320, 640 μM). A calibration curve was generated by measurement of varied concentrations (from 0.15 to 20 μM) of free Edans in a final volume of 50 μL reaction buffer. Initial velocities were determined from the linear section of the curve, and the corresponding relative fluorescence units per unit of time (ΔRFU/s) was converted to the amount of the cleaved substrate per unit of time (μM/s) by fitting to the calibration curve of free Edans.

Inner-filter effect corrections were applied for the kinetic measurements according to *(30)*. The fluorescence of the substrate (in RFU) dissolved in 50 μL final volume of reaction buffer at the corresponding concentrations used for the kinetic assay was measured and defined as f (substrate). Afterwards, 1 μL free Edans was added (final concentration: 5 μM) to each well, and the fluorescence reading was taken as f (substrate + Edans). Simultaneously, a reference value (in RFU) was measured with the same concentration of free Edans in 50 μL of reaction buffer, giving f (reference). The inner-filter correction at each substrate concentration was calculated according to the function:

corr% = (f (substrate + Edans) – f (substrate)) / f (reference) x 100%

The corrected initial velocity of the reaction was calculated as

$V = V_o / (corr\%)$.

V_o represents the initial velocity of each reaction.

As saturation could be achieved, kinetic constants (V_{max} and K_m) were derived by fitting the corrected initial velocity to the Michaelis-Menten equation, $V = V_{max} \times [S] / (K_m + [S])$ using GraphPad Prism 6.0 software. k_{cat}/K_m was calculated according to the equation, $k_{cat}/K_m = V_{max} / ([E] \times K_m)$. Triplicate experiments were performed for each data point, and the value was presented as mean ± standard deviation (SD).

Analytical ultracentrifugation

Sedimentation velocity experiments were carried out in a Beckman Coulter ProteomeLab XL-I analytical ultracentrifuge at 42,000 rpm and 20°C using an An-50 Ti rotor. Concentration profiles were measured with the absorption scanning optics at 230 nm using 3 or 12 mm standard double-sector centerpieces filled with 100 µL or 400 µL sample, respectively. SARS-CoV-2 or SARS-CoV M^{pro} was examined in a concentration range of 0.23 to 18.1 µM in a buffer containing 20 mM Tris, 150 mM NaCl, pH 7.3. Since in the observed monomer-dimer equilibrium, the peak positions did not change with loading concentration, the reaction is slow on the time scale of centrifugation *(31)* and the samples were allowed to equilibrate after dilution for about 23 hours at room temperature. For data analysis, a model for diffusion-deconvoluted differential sedimentation coefficient distributions (continuous c(s) distributions) implemented in the program SEDFIT *(32)* was used. Partial specific volumes, buffer density and viscosity were calculated from amino-acid and buffer composition, respectively, by the program SEDNTERP *(33)* and were used to correct experimental s-values to $s_{20,w}$.

Calculation of pocket volumes and preparation of structural figures

Binding-site (pocket) volumes were calculated by using UCSF Chimera *(34)*. Structural figures were prepared by using PyMol (Schrödinger LLC).

Inhibitor synthesis

Compound **11r** was synthesized according to *(6)*.

Scheme S1: Synthesis pathway to compounds 13a, 13b, 14b

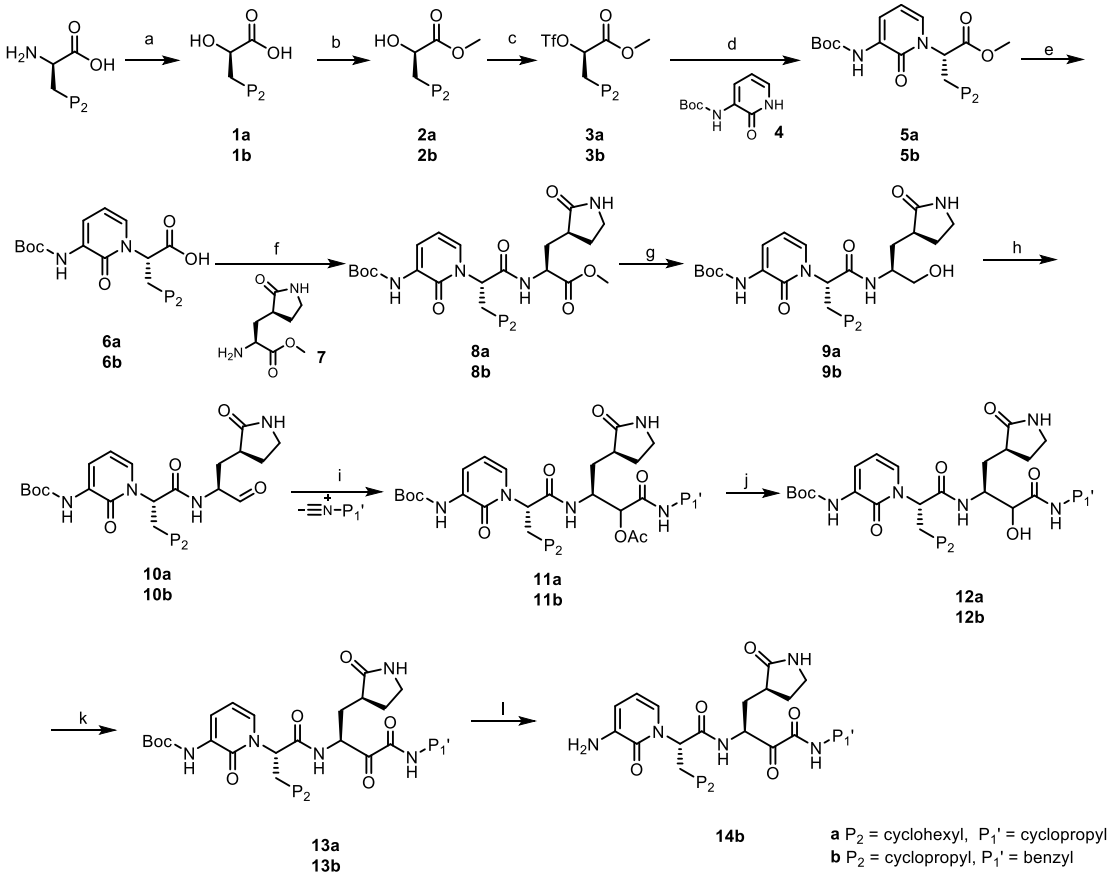

Reaction conditions: (a) $NaNO_2$, H_2SO_4, H_2O; (b) $SOCl_2$, MeOH; (c) Tf_2O, 2,6-lutidine, CH_2Cl_2; (d) NaH, THF; (e) LiOH, MeOH, H_2O; (f) HOBt, EDCI, CH_2Cl_2; (g) $NaBH_4$, MeOH; (h) DMP, $NaHCO_3$, CH_2Cl_2; (i) isocyanide, AcOH, CH_2Cl_2; (j) LiOH, MeOH, H_2O; (k) DMP, $NaHCO_3$, CH_2Cl_2; (l) 4M HCl, EA.

General procedure. Reagents were purchased from commercial sources and used without purification. HSGF 254 (0.15 - 0.2 mm thickness) was used for analytical thin-layer chromatography (TLC). All products were characterized by their NMR and MS spectra. ^{1}H NMR spectra were recorded on 300-MHz instruments. Chemical shifts are reported in parts per million (ppm, δ) down-field from tetramethylsilane. Proton coupling patterns are described as singlet (s), doublet (d), triplet (t), multiplet (m), and broad (br). Optical rotation was recorded by using a WZZ-2S polarimeter (Shanghai Precision Instruments). Mass spectra were recorded using an ESI ion-trap HCT Ultra (Bruker). HPLC spectra were recorded by an LC20A (Shimadzu Corporation) with Shim-pack GIST C18 (5 μm, 4.6 x 150 mm) with three solvent systems (methanol/water, methanol/0.1% HCOOH in water or methanol/0.1% ammonia in water). Purity was determined by reversed-phase HPLC and was ≥95% for **13a**, **13b** and **14b**.

Synthesis of compound 1

A solution of (*R*)-2-amino-3-cyclohexylpropanoic acid (7.74 mmol) or (*R*)-2-amino-3-cyclopropylpropanoic acid in 2N H_2SO_4 (15 mL) was stirred at 0°C. Then, $NaNO_2$ (5.34 g, 77.4 mmol) in H_2O (6 mL) was added dropwise to the reaction. The mixture was stirred for 3 h at 0°C and then allowed to warm to 20°C and stirred at 20°C for 16 h. The mixture was extracted with MTBE (50 mL). The combined organic phase was dried over anhydrous Na_2SO_4 and concentrated under vacuum to give compound **1** (as a colorless oil, 50-75% yield) without further purification.

Synthesis of compound 2

$SOCl_2$ (0.8 mL, 11.34 mmol) was added dropwise to the solution of compound **1** (5.72 mmol) in MeOH (20 mL) at 0°C. Then the mixture was stirred for 1.5 h at 20°C. The mixture was evaporated in vacuum and purified by chromatography on silica gel (PE/EA = 1/1) to give compound **2** (as colorless oil, 30-59 % yield).

M***ethyl (R)-3-cyclohexyl-2-hydroxypropanoate*** **2a**:

^{1}H NMR (300 MHz, $CDCl_3$) δ 4.39-4.34 (m, 1H), 3.82 (s, 3H), 1.82-1.48 (m, 8H), 1.29-1.12 (m, 4H), 1.00-0.85 (m, 2H).

Methyl (R)-3-cyclopropyl-2-hydroxypropanoate **2b**:

^{1}H NMR (300 MHz, $CDCl_3$) δ 4.35 (dd, J_1 = 9.0 Hz, J_2 = 4.2 Hz, 1H), 3.80 (s, 3H), 1.81-1.72 (m, 2H), 0.92-0.68 (m, 1H), 0.50-0.43 (m, 2H), 0.15-0.05 (m, 2H).

Synthesis of compound 3

Compound **2** (5.32 mmol) was dissolved in DCM (10 mL) and cooled to 0°C. 2,6-lutidine (1.5 mL, 13.26 mmol) and Tf_2O (3.3 g, 11.87 mmol) were added successively. The mixture was stirred for 30 min at 0°C. The mixture was extracted with MTBE after washing with a mixture of brine and 1N HCl (3:1 v/v), then dried over anhydrous Na_2SO_4, and evaporated to give compound **3** (as a brown oil, yield 82%) without further purification.

Synthesis of compound 5

Tert-butyl (2-oxo-1,2-dihydropyridin-3-yl)carbamate (379 mg, 1.8 mmol) was dissolved in THF (15 mL). NaH (115 mg, 2.80 mmol, 60% in oil) was added at 0°C and then stirred for 30 min. Then compound **3** (515 mg, 1.86 mmol) in THF (10 mL) was added. The mixture was stirred for 20 h at 25 °C. The mixture was evaporated in vacuum and purified by chromatography on silica gel (PE to EA) to give compound **5** (56-60% yield) as light yellow solid.

Methyl (S)-2-(3-((tert-butoxycarbonyl)amino)-2-oxopyridin-1(2H)-yl)-3-cyclohexyl propanoate 5a:

^{1}H NMR (300 MHz, DMSO-d_6) δ 7.82-7.76 (m, 2H), 7.35 (dd, J_1 = 7.5 Hz, J_2 = 1.5 Hz, 1H), 6.30 (t, J = 7.5 Hz, 1H), 5.35 (dd, J_1 = 11.1 Hz, J_2 = 4.5 Hz, 1H), 3.56 (s, 3H), 2.10-1.88 (m, 2H), 1.78-1.72 (m, 1H), 1.65-1.44 (m, 13H), 1.14-0.82 (m, 6H). ESI-MS (*m*/*z*): 379 $[M + H]^+$.

Methyl (S)-2-(3-((tert-butoxycarbonyl)amino)-2-oxopyridin-1(2H)-yl)-3-cyclopropyl propanoate 5b:

^{1}H NMR (300 MHz, DMSO-d_6) δ 7.83-7.78 (m, 2H), 7.35 (dd, J_1 = 7.2 Hz, J_2 = 1.5 Hz, 1H), 6.30 (t, J = 7.2 Hz, 1H), 5.36 (dd, J_1 = 10.8 Hz, J_2 = 4.5 Hz, 1H), 3.57 (s, 3H), 1.81-1.62 (m, 2H), 1.48 (s, 9H), 0.55-0.48 (m, 1H), 0.34-0.29 (m, 2H), 0.15-0.12 (m, 1H), 0.04-0.01 (m, 1H). ESI-MS (*m*/*z*): 337 $[M + H]^+$.

Synthesis of compound 6

Compound **5** (1.65 mmol) was dissolved in MeOH (15 mL) and H_2O (3 mL). $LiOH.H_2O$ (139 mg, 3.31 mmol) was added. The mixture was stirred at 20°C for 1 h. Then, the mixture was adjusted to pH=6~7 with 1N HCl. Subsequently, the reaction was evaporated under vacuum and purified by

chromatography on silica gel (DCM/MeOH = 10/1) to give compound **6** (452 mg, 84% yield) as light yellow solid.

(S)-2-(3-((tert-butoxycarbonyl)amino)-2-oxopyridin-1(2H)-yl)-3-cyclohexylpropanoic acid 6a:

^{1}H NMR (300 MHz, DMSO-d_6) δ 13.12 (s, 1H), 7.83-7.77 (m, 2H), 7.35 (dd, J_1 = 7.2 Hz, J_2 = 1.5 Hz, 1H), 6.30 (t, J = 7.2 Hz, 1H), 5.35 (dd, J_1 = 10.8 Hz, J_2 = 4.5 Hz, 1H), 2.10-1.92 (m, 2H), 1.78-1.69 (m, 1H), 1.65-1.52 (m, 4H), 1.47 (s, 9H), 1.13-0.82 (m, 6H). ESI-MS (*m*/*z*): 365 $[M + H]^+$.

(S)-2-(3-((tert-butoxycarbonyl)amino)-2-oxopyridin-1(2H)-yl)-3-cyclopropylpropanoic acid 6b:

^{1}H NMR (300 MHz, DMSO-d_6) δ 13.11(s, 1H), 7.81-7.77 (m, 2H), 7.36 (dd, J_1 = 6.9 Hz, J_2 = 1.5 Hz, 1H), 6.30 (t, J = 6.9 Hz, 1H), 5.35 (dd, J_1 = 10.5 Hz, J_2 = 4.5 Hz, 1H), 1.80-1.69 (m, 2H), 1.47 (s, 9H), 0.53-0.48 (m, 1H), 0.32-0.29 (m, 2H), 0.14-0.11 (m, 1H), 0.03-0.00 (m, 1H). $[\alpha]^{20}_D$ -22.4 (c 1.0 g/100 mL, MeOH), ESI-MS (*m*/*z*): 323 $[M + H]^+$.

Synthesis of compound 7

Compound 7 was synthesized according to *(35)*.

Synthesis of compound 8

HOBt (245 mg, 1.82 mmol) and EDCI (349 mg, 1.82 mmol) were added to the solution of compound **6** (1.65 mmol) in DCM (20 mL). The mixture was stirred for 1 h at 0°C. Then compound **7,** methyl (S)-2-amino-3-((S)-2-oxopyrrolidin-3-yl) propanoate (307 mg, 1.65 mmol), was added, and the mixture was adjusted to pH = 9 with Et_3N. The mixture was stirred at 0°C for 24 h. Then, the reaction was concentrated and purified by chromatography on silica gel (DCM/MeOH=20/1) to give compound **8** (59-67% yield) as light yellow solid.

Methyl (S)-2-((S)-2-(3-((tert-butoxycarbonyl)amino)-2-oxopyridin-1(2H)-yl)-3-cyclohexylpropanamido)-3-((S)-2-oxopyrrolidin-3-yl)propanoate 8a:

ESI-MS (*m*/*z*): 533 $[M + H]^+$

Methyl (S)-2-((S)-2-(3-((tert-butoxycarbonyl)amino)-2-oxopyridin-1(2H)-yl)-3-cyclopropylpropanamido)-3-((S)-2-oxopyrrolidin-3-yl)propanoate 8b:

^{1}H NMR (300 MHz, DMSO-d_6) δ 9.00-8.92 (m, 1H), 7.81-7.77 (m, 2H), 7.37-7.34 (m, 1H), 6.30 (t, *J* = 7.2 Hz, 1H), 5.77 (dd, J_1 = 10.8 Hz, J_2 = 4.5 Hz, 1H), 4.54-4.45 (m, 1H), 3.74 (s, 3H), 3.37-3.29 (m, 2H), 2.35-2.25 (m, 2H), 1.90-1.71 (m, 5H), 1.46 (s, 9H), 0.51-0.46 (m, 1H), 0.32-0.29 (m, 2H), 0.15-0.11 (m, 1H), 0.04-0.00 (m, 1H). ESI-MS (*m*/*z*): 491 $[M + H]^+$.

Synthesis of compound 9

$NaBH_4$ (200 mg, 5.3 mmol) was added to a solution of compound **8** (0.53 mmol) in MeOH (6 mL). The mixture was stirred at 25°C for 3 h. The reaction was concentrated and purified by chromatography on silica gel (DCM/MeOH=10/1) to give compound **9** (49%, as off-white solid).

Tert-butyl (1-((S)-3-cyclohexyl-1-(((S)-1-hydroxy-3-((S)-2-oxopyrrolidin-3-yl)propanyl-2-)amino)-1-oxopropan-2-yl)-2-oxo-1,2-dihydropyridin-3-yl)carbamate 9a:

ESI-MS (*m*/*z*): 505 $[M + H]^+$.

Tert-butyl (1-((S)-3-cyclopropyl-1-(((S)-1-hydroxy-3-((S)-2-oxopyrrolidin-3-yl)propan-2-yl)amino)-1-oxopropan-2-yl)-2-oxo-1,2-dihydropyridin-3-yl)carbamate 9b:

ESI-MS (*m*/*z*): 463 $[M + H]^+$.

Synthesis of compound 10

Dess-Martin periodinane (116 mg, 0.27 mmol) and $NaHCO_3$ (8 mg, 0.09 mmol) were added to a solution of compound **9** (0.26 mmol) in DCM (15 mL). The mixture was stirred at 20ºC for 1 h. The reaction was concentrated and purified by chromatography on silica gel (DCM/MeOH=20/1) to give compound **10** (83 - 90% yield) as off-white solid.

Tert-butyl (1-((S)-3-cyclohexyl-1-oxo-1-(((S)-1-oxo-3-((S)-2-oxopyrrolidin-3-yl)propan-2-yl)amino)propan-2-yl)-2-oxo-1,2-dihydropyridin-3-yl)carbamate 10a:

ESI-MS (*m*/*z*): 503 $[M + H]^+$.

Tert-butyl (1-((S)-3-cyclopropyl-1-oxo-1-(((S)-1-oxo-3-((S)-2-oxopyrrolidin-3-yl)-propan-2-yl) amino)propan-2-yl)-2-oxo-1,2-dihydropyridin-3-yl)carbamate 10b:

^{1}H NMR (300 MHz, DMSO-d_6) δ 9.40 (d, J = 7.8 Hz, 1H), 8.97 (dd, J_1 = 14.1 Hz, J_2 = 7.2 Hz, 1H), 7.79-7.73 (m, 2H), 7.35-7.32 (m, 1H), 6.30 (t, J = 7.5 Hz, 1H), 5.69-5.62 (m, 1H), 4.48-4.42 (m, 1H), 3.20-3.10 (m, 2H), 2.32-2.15 (m, 2H), 1.88-1.66 (m, 5H), 1.46 (s, 9H), 0.55-0.47 (s, 1H), 0.36-0.29 (m, 2H), 0.14-0.11 (m, 1H), 0.04-0.00 (m, 1H). ESI-MS (*m*/*z*): 461 $[M + H]^+$.

Synthesis of compound 11 (general method)

Acetic acid (26 mg, 0.44 mmol) and isocyanide (0.22 mmol) were added to the solution of compound **10** (0.22 mmol) in DCM (15 mL). The mixture was stirred at 20ºC for 24 h. The reaction was concentrated and purified by chromatography on silica gel (DCM/MeOH=20/1) to give compound **11** (57-65% yield) as off-white solid.

Synthesis of compound 12 (general method)

Compound **11** (0.13 mmol) was dissolved in MeOH (15 mL) and H_2O (3 mL). $LiOH.H_2O$ (11 mg, 0.26 mmol) was added. The mixture was stirred at 20°C for 20 min. The mixture was adjusted to pH=6~7 with 1N HCl. The reaction was concentrated and purified by chromatography on silica gel (DCM/MeOH=10/1) to give compound **12** (90-95% yield) as off-white solid.

Synthesis of compound 13 (general method)

Compound **12** (0.115 mmol) was dissolved in DCM (15 mL). Dess-Martin periodinane (58 mg, 0.14 mmol) and $NaHCO_3$ (4 mg, 0.05 mmol) were added. The mixture was stirred at 25°C for 1 h. The reaction was concentrated and purified by chromatography on silica gel (DCM/MeOH=10/1) to give compound **13** (69-80% yield) as off-white solid.

Tert-butyl (1-((S)-3-cyclohexyl-1-(((S)-4-(cyclopropylamino)-3,4-dioxo-1-((S)-2-oxopyrrolidin-3-yl)butan-2-yl)amino)-1-oxopropan-2-yl)-2-oxo-1,2-dihydropyridin-3-yl)carbamate 13a:

^{1}H NMR (300 MHz, $CDCl_3$) δ 8.78-8.50 (m, 1H), 8.01-7.92 (m, 1H), 7.65 (d, *J* = 7.5 Hz, 1H), 7.10-6.90 (m, 2H), 6.35-6.14 (m, 2H), 5.85-5.75 (m, 1H), 5.25-5.10 (m, 1H), 3.24-3.13 (m, 2H), 2.75-2.71 (m, 1H), 2.49-2.20 (m, 1H), 2.10-1.81 (m, 3H) 1.80-1.52 (m, 7H), 1.50-1.46 (m, 10H), 1.25-1.01 (m, 4H), 1.00-0.73 (m, 4H), 0.56-0.51 (m, 2H). ^{13}C NMR (300 MHz, DMSO-d_6) δ 196.35, 178.43, 170.14, 162.35, 157.01, 152.67, 128.85, 128.35, 120.49, 105.46, 80.60, 54.66, 52.98, 39.91, 38.35, 34.06, 33.32, 31.85, 31.52, 28.37, 27.62, 26.39, 26.11, 25.89, 22.95, 5.87. $[\alpha]^{20}_D$ -36.4 (c 0.5 g/100 mL, MeOH), ESI-MS (*m*/*z*): 586 $[M + H]^+$.

Tert-butyl (1-((S)-1-(((S)-4-(benzylamino)-3,4-dioxo-1-((S)-2-oxopyrrolidin-3-yl)-butan-2-yl)amino)-3-cyclopropyl-1-oxopropan-2-yl)-2-oxo-1,2-dihydropyridin-3-yl)carbamate 13b:

^{1}H NMR (300 MHz, DMSO-d_6) δ 9.25 (d, J = 5.4 Hz, 1H), 9.00 (dd, J_1 = 14.1 Hz, J_2 = 7.2 Hz, 1H), 7.79-7.69 (m, 3H), 7.35-7.22 (m, 5H), 6.30-6.24 (m, 1H), 5.69-5.61 (m, 1H), 4.97 (s, br, 1H), 4.29 (s, 2H), 3.17-3.09 (m, 2H), 2.30-2.15 (m, 2H), 1.91-1.62 (m, 5H), 1.46 (s, 9H), 0.52-0.47 (m, 1H), 0.33-0.29 (m, 2H), 0.14-0.09 (m, 1H), 0.02- -0.01 (m, 1H). ^{13}C NMR (300 MHz, DMSO-d_6) δ 196.68, 178.45, 169.90, 161.22, 157.24, 152.67, 138.95, 129.24, 128.76, 128.58, 127.80, 127.44, 120.41, 105.37, 80.59, 58.30, 53.24, 42.52, 39.89, 38.28, 35.01, 31.61, 28.38, 27.58, 7.96, 4.90, 4.05. $[\alpha]^{20}_{D}$ -30.8 (c 0.5 g/100 mL, MeOH). ESI-MS (*m*/*z*): 594 $[M + H]^+$.

Synthesis of (S)-3-((S)-2-(3-amino-2-oxopyridin-1(2H)-yl)-3-cyclopropylpropan-amido)-N-benzyl-2-oxo-4-((S)-2-oxopyrrolidin-3-yl)butanamide 14b

Compound **13b** (0.11 mmol) was added to the solution 4N HCl/EA (30 mL). The mixture was stirred at 25°C for 1 h. Then, the solvent was removed under reduced pressure, and to the residue, ether (2 mL) was added while stirring. The white solid was precipitated. The mixture was filtered and the filter cake was washed with diethyl ether (1 mL) to afford compound **14b** as off-white solid (54% yield).

^{1}H NMR (300 MHz, DMSO-d_6) δ 9.25 (d, J = 5.4 Hz, 1H), 9.06 (dd, J_1 = 14.1 Hz, J_2 = 7.2 Hz, 1H), 7.73-7.59 (m, 2H), 7.34-7.21 (m, 5H), 6.30 (t, J = 7.5 Hz, 1H), 5.75-5.64 (m, 1H), 5.00 (s, br, 1H), 4.30 (s, 2H), 3.17-3.09 (m, 2H), 2.26-2.12 (m, 2H), 1.99-1.63 (m, 5H), 0.51-0.46 (m, 1H), 0.34-0.30 (m, 2H), 0.15-0.13 (m, 1H), 0.02- -0.02 (m, 1H). ^{13}C NMR (300 MHz, DMSO-d_6) δ 196.59, 178.42, 169.87, 161.13, 158.23, 140.97, 138.95, 133.42, 128.78, 128.64, 127.82, 127.46, 104.93, 57.95, 53.23, 42.54, 40.52, 38.33, 36.18, 31.62, 27.62, 8.05, 5.00, 3.94. ESI-MS (*m*/*z*): 494 $[M + H]^+$.

Diastereomeric purity

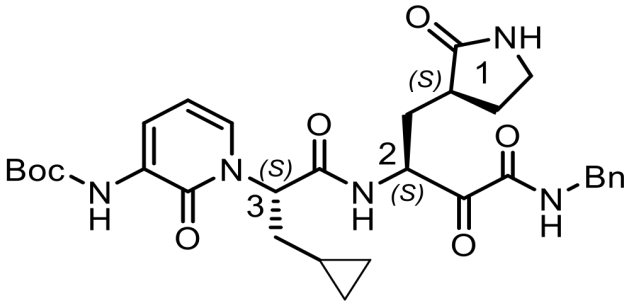

13b

Fig. S1: Stereocenters of compound 13b

Compound **7** was synthesized according to the literature *(35)* and should have the *S* configuration at both stereocenters, as it has been shown that the asymmetric dianionic cyanomethylation of N-Boc L-(+)-glutamic acid dimethyl ester is highly stereospecific *(35)*. We observed partial racemization of compound **8** at the P2 α-carbon, which may occur upon step d or step f (see Scheme S1). However, our target, the *S*-diastereomer of **8**, is the main product and can be separated from the *R*-diastereomer by chromatography on silica gel (DCM/MeOH = 40/1), (TLC rf: *R*-isomer 0.40, *S*-isomer 0.38 on silica gel, DCM/MeOH=20/1). The following conditions of steps g, h, i, j, k are mild and are unlikely to lead to racemization at P1 and P2. Furthermore, the diastereomers can be monitored by TLC during the reaction, and we just collected the main components of the mixture during flash chromatography purification, thereby also reducing the risk of impurity of the final target. Notably, we obtained two diastereomers of compounds **11** and **12**, which were easily separated by flash chromatography on silica gel (TLC, compound **12**, isomer 1: 0.58, isomer 2: 0.35, DCM/MeOH = 10/1, ratio 1 to 1). We tried the oxidation of the two isomers independently, and

found that they finally led to the same compounds **13a,b**. The structure of **13b** is confirmed by the crystal structure of its complex with the SARS-CoV-2 M^{pro}.

^{1}H and ^{13}C NMR spectra

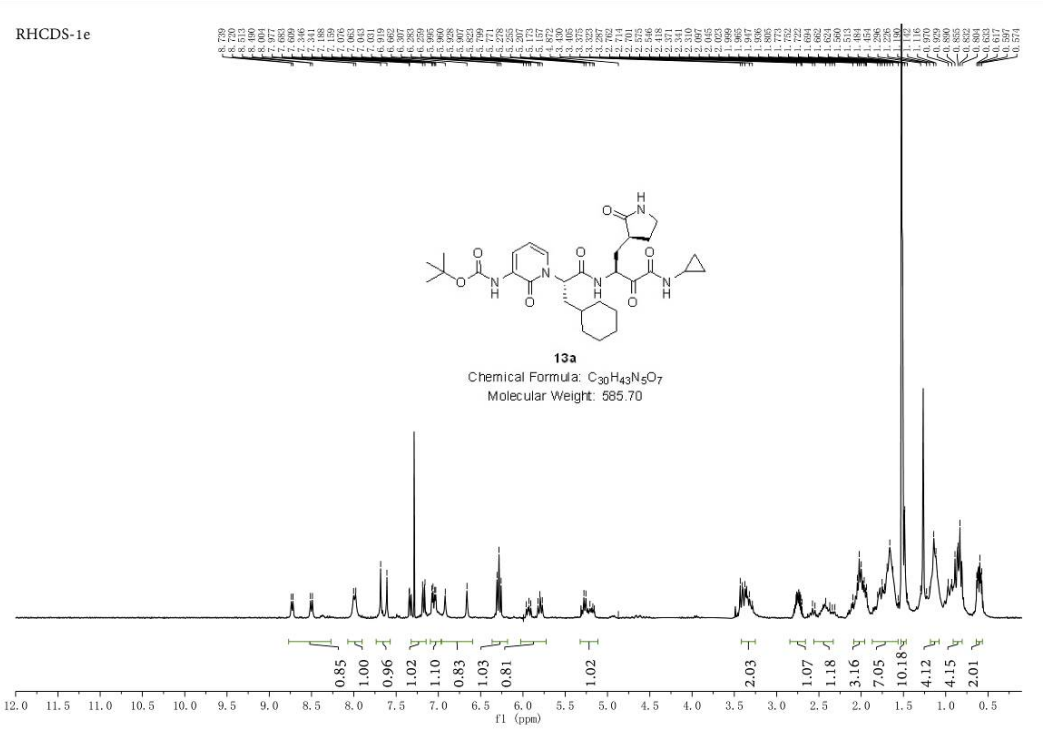

Fig. S2: ^{1}H NMR spectrum of 13a

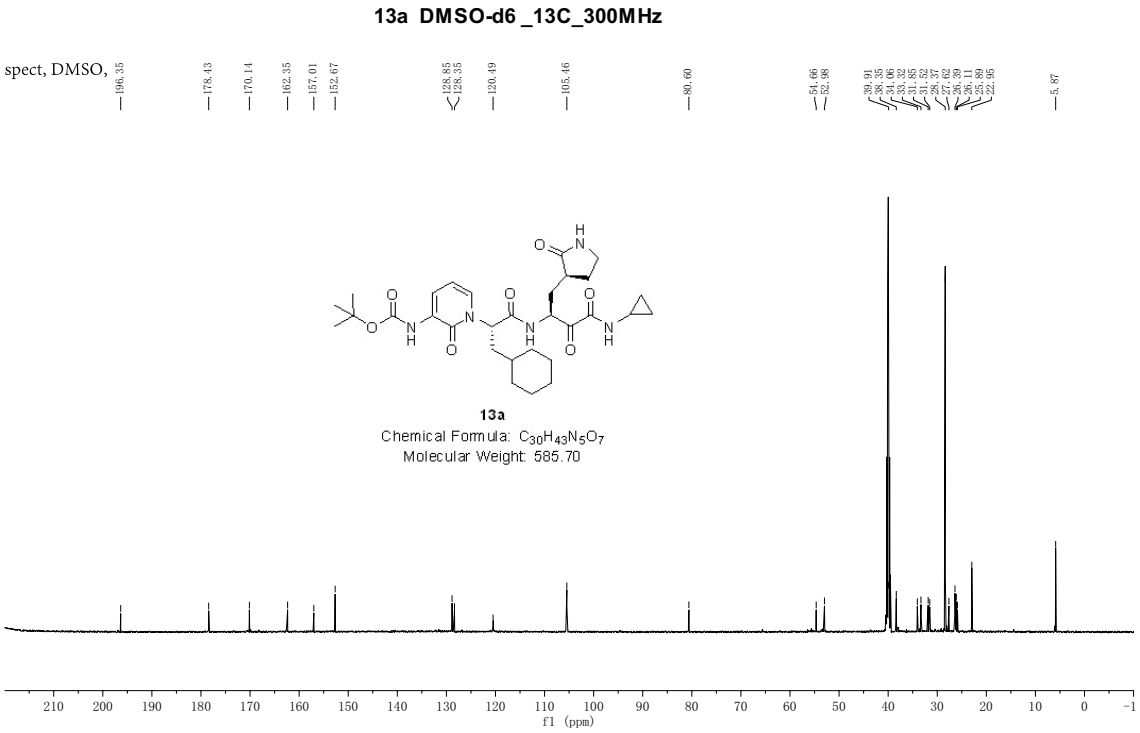

Fig. S3: ^{13}C NMR spectrum of 13a

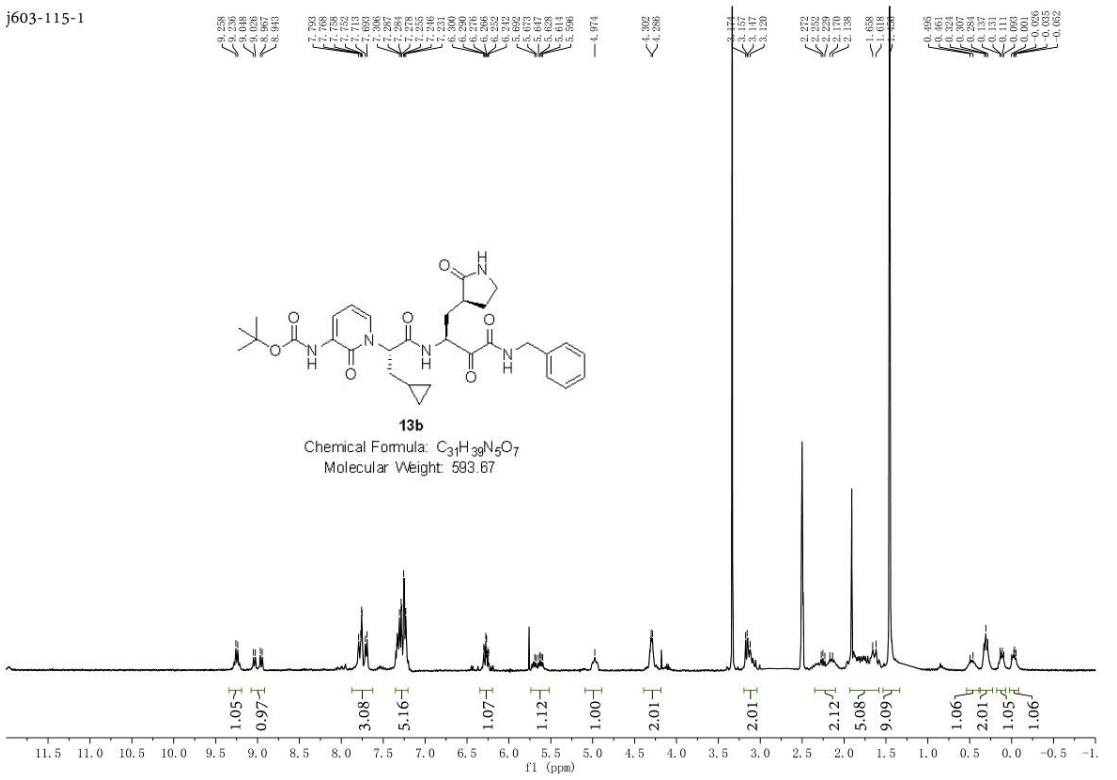

Fig. S4: ^{1}H NMR spectrum of 13b

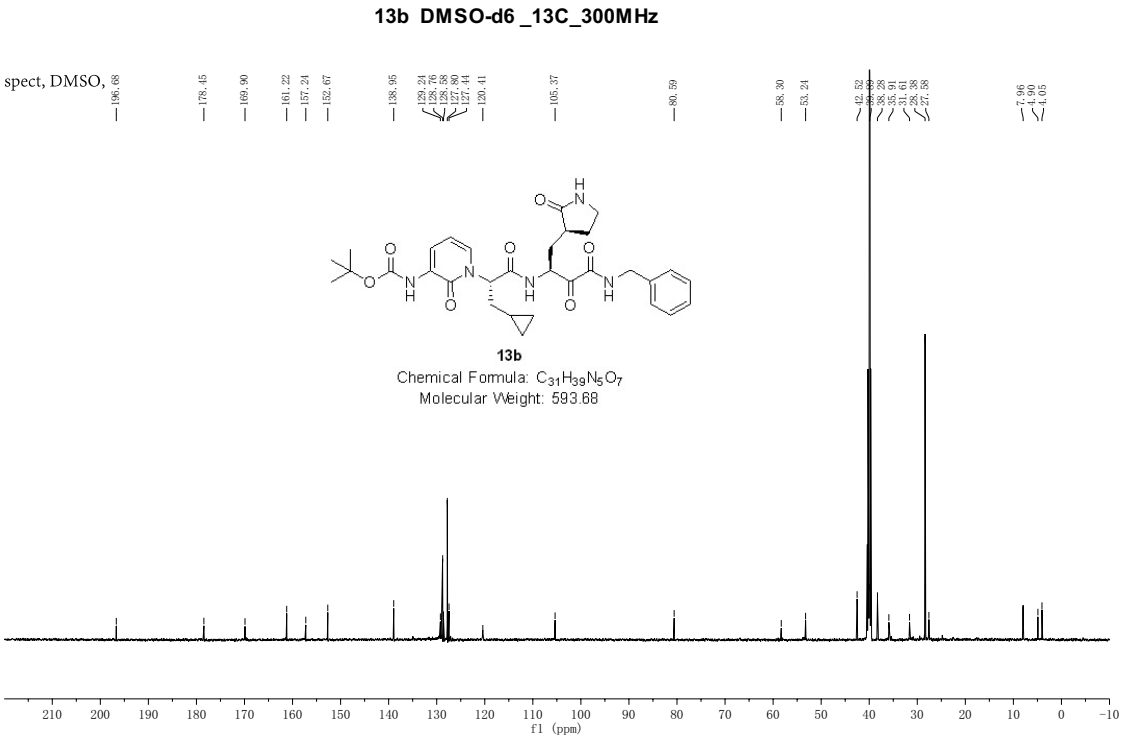

Fig. S5: ^{13}C NMR spectrum of 13b

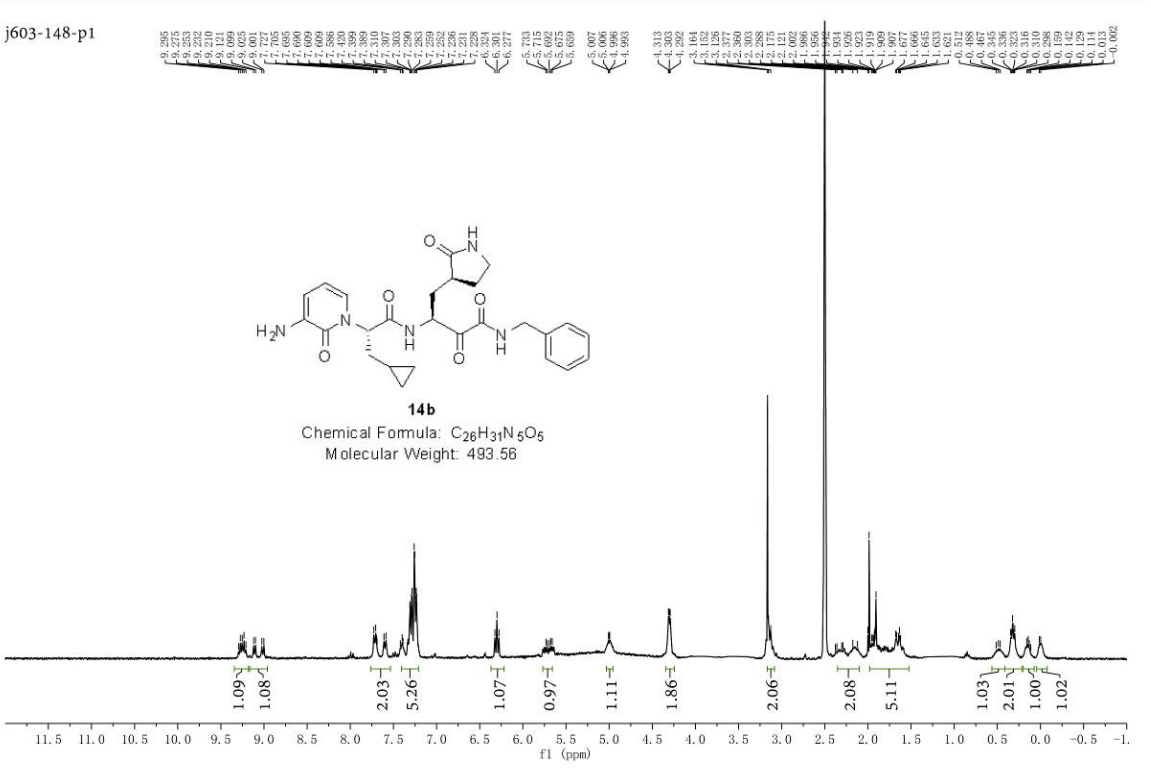

Fig. S6: ^{1}H NMR spectrum of 14b

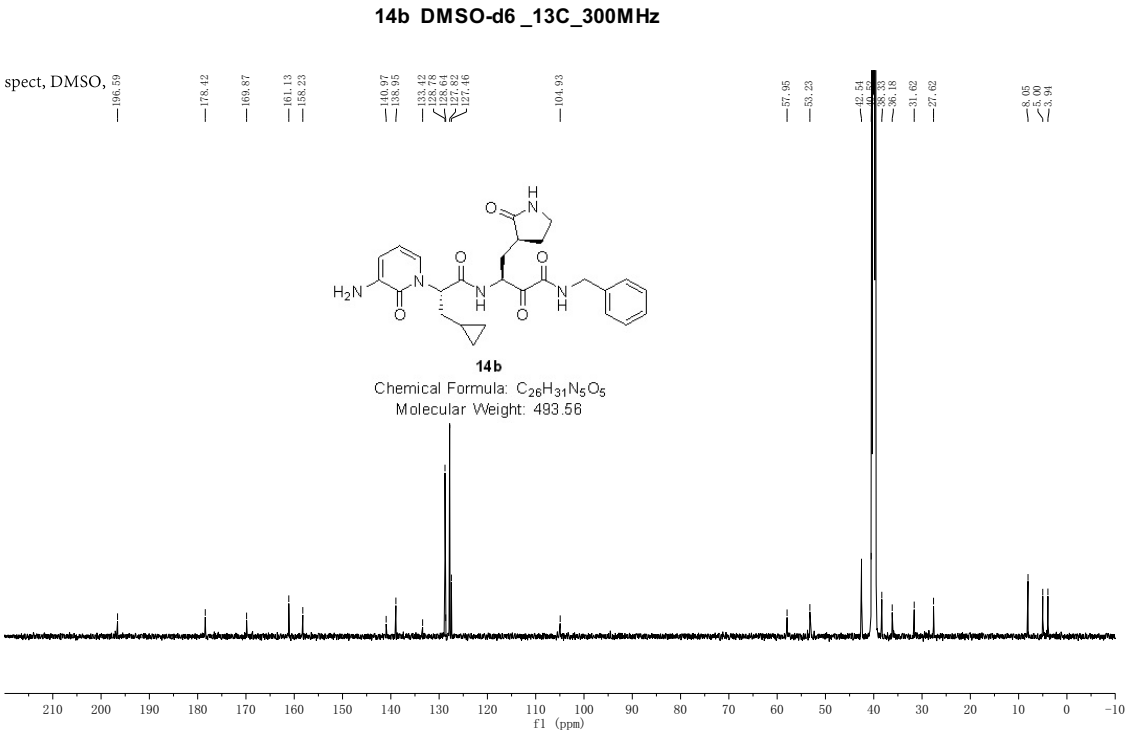

Fig. S7: ^{13}C NMR spectrum of 14b

Determination of inhibition of SARS-CoV-2 M^{pro} by 11r, 13a, and 13b

The same reaction buffer, substrate, and monitor equipment were employed as described in the paragraph on enzyme kinetics of SARS-CoV-2 and SARS-CoV M^{pro} (see above). Stock solutions of the compounds were prepared with 100% DMSO. For the determination of the IC_{50}, 0.5 μM of SARS-CoV-2 M^{pro} was incubated with **11r**, **13a**, or **13b** at various concentrations from 0 to 100 μM in reaction buffer at 37°C for 10 min. Afterwards, the FRET substrate at a final concentration of 20 μM was added to each well at a final total volume of 50 μL to initiate the reaction. The GraphPad Prism 6.0 software (GraphPad) was used for the calculation of the IC_{50} values. Measurements of inhibitory activities of the compounds were performed in triplicate and are presented as the mean ± SD.

SARS-CoV-2 infection experiments

Experiments with SARS-CoV-2 were performed under biosafety level 3 (BSL-3) conditions at the Institute of Virology, Philipps-University of Marburg, Germany. Calu-3 cells were infected with SARS-CoV-2 at a multiplicity of infection (MOI) of 0.05 diluted in DMEM/F12 without FCS at 37°C for 1 h. Cells were washed with DMEM/F12 with 10% FCS and supplemented with **13b** or **14b** in different concentrations. For solvent control, cells were only treated with DMSO. 24 h after infection (p.i.), cells were lysed and quantitative PCR was performed (based on a protocol published in *(36)*). For that, 5 µg of total RNA were analyzed with the QIAGEN OneStep RT-PCR Kit according to the manufacturer's instructions. Two independent biological replicates, each with two technical replicates, were performed.

Determination of absorption - distribution - metabolism - excretion (ADME) properties of compounds 13a and 13b

Plasma protein binding. Plasma protein binding was assessed using the rapid equilibrium device (RED) system from ThermoFisher. Compounds were dissolved in DMSO. Naproxene served as control as it shows high plasma protein binding. Compounds were diluted in murine plasma (from CD-1 mice, pooled) to a final concentration of 100 µM. Dialysis buffer and plasma samples were added to the respective chambers according the manufacturer's protocol. The RED plate was sealed with a tape and incubated at 37°C for 2 hours at 800 rpm on an Eppendorf MixMate® vortex-mixer. Then samples were withdrawn from the respective chambers. To 25 µL of each dialysis sample, 25 µL of plasma and to 25 µL of plasma sample, 25 µL of dialysis buffer was added. Then 150 µL ice-cold extraction solvent (acetonitrile/H_2O (90:10) containing 12.5 ng/mL caffeine as internal

standard) was added. Samples were incubated for 30 min on ice. Then samples were centrifuged at 4°C at 2270 x *g* for 10 min. Supernatants were transferred to Greiner V-bottom 96-well plates and sealed with a tape. The percentage of bound compound was calculated as follows:

(1) % free = (concentration buffer chamber / concentration plasma chamber) x 100%

% bound = 100% - % free.

Plasma stability. **13a** or **13b** dissolved in DMSO was added to mouse plasma (pH 7.4, 37°C) to yield a final concentration of 25 µM. In addition, procaine and procainamide (dissolved in DMSO) were added to mouse plasma (pH 7.4, 37°C) to yield a final concentration of 250 µM. Procaine served as positive control as it is unstable in mouse plasma. Procainamide served as negative control as it is stable in mouse plasma. The samples were incubated for 0 min, 15 min, 30 min, 60 min, 90 min, and 120 min at 37°C. At each time point, 7.5 µL of the respective sample was extracted with 22.5 µL methanol containing an internal standard for 5 min at 2000 rpm on a MixMate® vortex mixer (Eppendorf). Then samples were centrifuged for 2 min at 15.870 x *g* and the supernatants were transferred to HPLC-glass vials. 100 ng/mL glipizide was used as internal standard for HPLC-MS. Peak areas of each compound and of the internal standard were analyzed using the MultiQuant 3.0 software (AB Sciex). Peak areas of the respective compound were normalized to the internal standard peak area and to the respective peak areas at time point 0 min: (C/D)/(A/B) with A: peak area of the compound at time point 0 min, B: peak area of the internal standard at time point 0 min, C: peak area of the compound at the respective time point, D: peak area of the internal standard at the respective time point. Every experiment was repeated independently at least three times.

Microsomal stability. S9 liver microsomes (mouse and human, ThermoFisher) were thawed slowly on ice. 20 mg/mL of microsomes, 2 µL of a 100 µM solution of **13a** or **13b** and 183 µL of 100 mM

phosphate buffer were incubated for 5 min at 37°C in a water bath. Reactions were initiated using 10 µL of 20 mM NADPH. Samples were incubated in three replicates at 37°C under gentle agitation at 150 rpm. At 0, 15, 30, and 60 min, reactions were terminated by the addition of 200 µL acetonitrile. Samples were vortexed and centrifuged at 2270 x *g* for 10 min at 4°C. The supernatants were transferred to 96-well Greiner V-bottom plates, sealed and analyzed according to the section HPLC-MS analysis below. Peak areas of the respective time point of **13a** or **13b** were normalized to the peak area at time point 0 min.

Solubility assays. First, a calibration curve was prepared with **13a** ranging from 2.5 to 500 µM. For determination of kinetic solubility, 0.5 mmol of **13a** was added to a 96-well plate in triplicates. 100 µL buffer of pH 7.4 was added to every replicate of **13a**. Samples were incubated at room temperature. At 15 min and 4 h, 10 µL were taken from every well and transferred to a new 96-well plate. Then 190 µL acetonitrile containing 12.5 ng/mL glipizide as internal standard was added. For thermodynamic solubility, 0.5 mmol of **13a** were added to a glass vial. Buffer of pH 7.4 was added and samples were incubated at 20°C for 24, 48, and 72 h under agitation (120 rpm). At the respective time points, 10 µL of every replicate were taken and transferred to a new 96-well plate. 190 µL acetonitrile containing 12.5 ng/mL glipizide as internal standard was added. All samples were centrifuged for 10 min at 12°C and 2270 x *g*, supernatants were transferred to a new Greiner 96-well V-bottom plate. All samples were analyzed according to the section HPLC-MS analysis below.

***HPLC-MS analysis*.** Samples were analyzed using an Agilent 1290 Infinity II HPLC system coupled to an AB Sciex QTrap 6500plus mass spectrometer. LC conditions were as follows: column:

Agilent Zorbax Eclipse Plus C18, 50x2.1 mm, 1.8 µm; temperature: 30°C; injection volume: 5 µL for plasma, 10 µL for urine, lung and BALF; 10 µL for samples from plasma stability, metabolic stability, plasma protein binding, and solubility assays; flow rate: 700 µL/min; solvent A: water + 0.1 % formic acid; solvent B: 95% acetonitrile/5% H_2O + 0.1% formic acid; gradient: 99% A at 0 min, 99% A until 0.1 min, 99% - 0% A from 0.1 min to 5.5 min, 0% A until 6.0 min, 0% - 99 % A from 6.0 min to 6.4 min, 99 % A until 6.5 min. Mass transitions for controls and **13a** as well as **13b** are given in Table S1.

Table S1. Mass transitions of compounds

	Q1 mass	Q3 mass	Time [msec]	DP [volts]	CE [volts]	CXP [volts]
Naproxene	231.106	185.1	50	80	19	10
	231.106	170.2	50	80	33	12
Caffeine	195.024	138.0	30	80	25	14
	195.024	110.0	30	80	31	18
13a	608.228	508.2	30	1	39	28
	608.228	313.1	30	1	53	34
13b	594.156	305.1	30	31	19	18
	594.156	249.0	30	31	35	12
Glipizide	444.027	318.9	30	-200	-38	-12
	444.027	170.0	30	-200	-38	-12
Procaine	235.744	163.0	30	80	21	18
	235.744	120.0	30	80	39	12
Procainamide	236.773	100.0	30	80	21	12
	236.773	120.0	30	80	31	14

Determination of pharmacokinetic properties

Mice. For pharmacokinetic experiments, outbred male CD-1 mice (Charles River), 4 weeks old, were used. The animal studies were conducted in accordance with the recommendations of the European Community (Directive 86/609/EEC, 24 November 1986). All animal procedures were performed in strict accordance with the German regulations of the Society for Laboratory Animal Science (GV-SOLAS) and the European Health Law of the Federation of Laboratory Animal

Science Associations (FELASA). Animals were excluded from further analysis if sacrifice was necessary according to the human endpoints established by the ethical board. All experiments were approved by the ethical board of the Niedersächsisches Landesamt für Verbraucherschutz und Lebensmittelsicherheit, Oldenburg, Germany (LAVES; permit nos. 33.19-42502-04-15/1857 and 33.19-42502-04-18/2892).

***Pharmacokinetic (PK) study*.** **13a** was dissolved in olive oil and water containing lecithin (40 mg lecithin dissolved in 800 µL of water). **13b** was dissolved in DMSO, Kolliphor EL®, Tween 80 ®, sodium citrate and water. Mice were administered **13a** subcutaneously (s.c.) at 20 mg/kg and **13b** at 3 mg/kg sc. For **13a**: About 20 µL of whole blood was collected serially from the lateral tail vein at time points 0.25, 0.5, 1, 2, 4, and 8 h post administration. After 24 h, mice were sacrificed and blood was collected from the heart. For **13b**: Mice were sacrificed and blood was collected from the heart at time points 0.25, 0.5, 1, 2, 4, 8, and 24 h post administration. Whole blood was collected into Eppendorf tubes coated with 0.5 M EDTA and immediately spun down at 15,870 x *g* for 10 min at 4°C. The plasma was transferred into a new Eppendorf tube and then stored at −80°C until analysis. For **13b**: Lungs were aseptically removed at each time point, homogenized and compound levels were analyzed using HPLC-MS/MS.

***PK sample preparation and analysis*.** First, a calibration curve was prepared by spiking different concentrations of **13a** or **13b** into mouse plasma, mouse urine, murine broncheo-alveolar lavage fluid (BALF), or homogenized lung from CD-1 mice. Caffeine was used as an internal standard. In addition, quality control samples (QCs) were prepared for **13a** and **13b**, respectively, in plasma, urine, BALF, and homogenized lung. The following extraction procedures were used: 7.5 µL of a

plasma sample or 10 µL of a urine sample (calibration samples, QCs or PK samples) was extracted with 25 µL of acetonitrile containing 12.5 ng/mL of caffeine as internal standard for 5 min at 2000 rpm on an Eppendorf MixMate® vortex mixer; 50 µL of a lung sample (concentration adjusted to 50 mg/mL, calibration samples, QCs or PK samples) was extracted with 50 µL of acetonitrile containing 12.5 ng/mL caffeine as internal standard for 5 min at 2000 rpm on an Eppendorf MixMate® vortex mixer. BALF samples were prepared as follows: 300 µL methanol were added to 200 µL of a BALF sample (calibration samples, QCs or PK samples) and samples were evaporated to dryness in an Eppendorf concentrator. Then, 80 µL of water were added to every dry sample and incubated for 10 min at 2000 rpm on an Eppendorf MixMate® vortex mixer. Then, 20 µL of acetonitrile containing 125 ng/mL caffeine were added and samples incubated for another 5 min at 2000 rpm on an Eppendorf MixMate® vortex mixer. Then samples were spun down at 15,870 x *g* for 10 min. Supernatants were transferred to standard HPLC-glass vials as described in the section HPLC-MS analysis above. Peaks of PK samples were quantified using the calibration curve. The accuracy of the calibration curve was determined using QCs independently prepared on different days. PK parameters were determined using a non-compartmental analysis with PKSolver *(37)*.

Supplementary Results

1. Amino-acid sequence alignment of SARS-CoV-2 and SARS-CoV main proteases

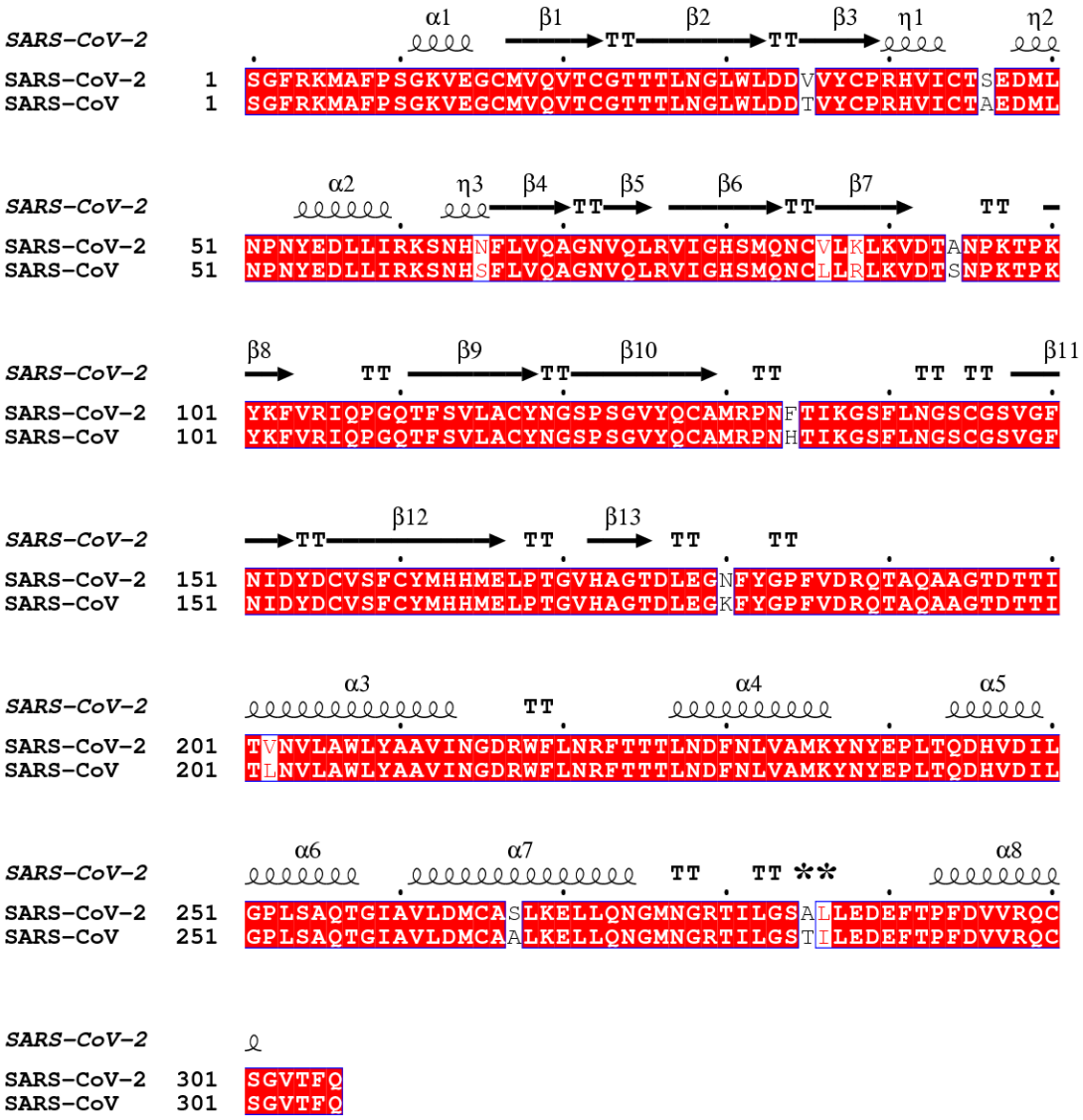

Fig. S8: Sequence alignment of the main proteases of SARS-CoV-2 and SARS-CoV.

Identical residues are indicated by red background. Residues 285 and 286 (see text) are highlighted by asterisks. Secondary structure as found in the crystal structure of SARS-CoV-2 M^{pro} is indicated above the amino-acid sequences. α = α-helix, β = β-strand, η - 3_{10}-helix, TT = turn.

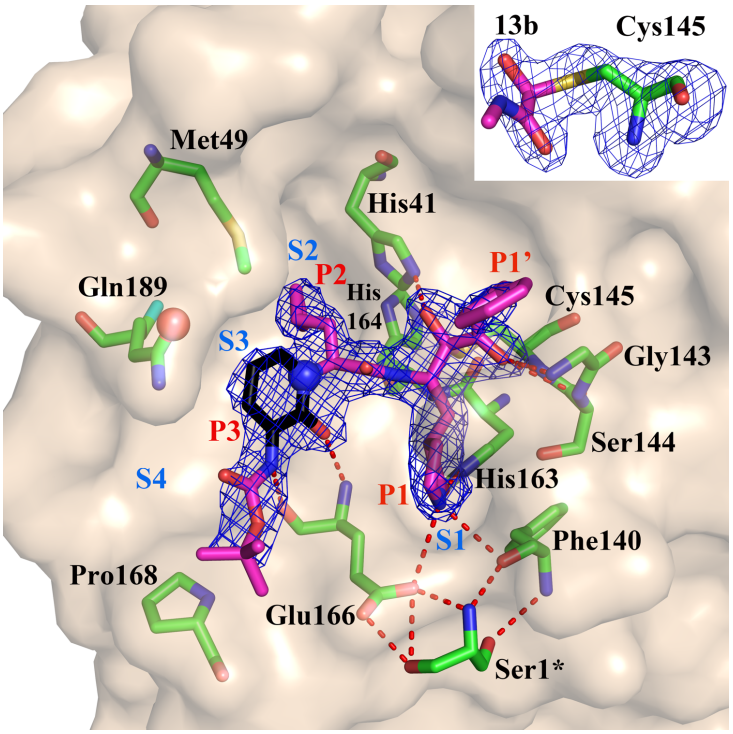

Fig. S9: As in Fig. 2 of the main text, but with the two atoms prevented from interacting (pyridone amide N and Gln189) indicated by spheres (blue for the amide nitrogen, red for Gln189 side-chain oxygen).

2. Analysis of the oligomerization behavior of SARS-CoV-2 and SARS-CoV M^{pro} by analytical ultracentrifugation

In order to examine the oligomerization behavior of SARS-CoV-2 M^{pro}, the protein was analyzed at concentrations of 0.23, 0.45, 0.60, 0.91, 1.00, 1.81, 2.50, 3.62, 4.53, 5.00, 7.50, 10.0, 12.5, and 18.1 µM in sedimentation velocity experiments in an analytical ultracentrifuge. It can be clearly seen that a monomer-dimer equilibrium is observed, whereupon the monomer sediments at $s_{20,w}$ = 2.9 S and the dimer at $s_{20,w}$ = 4.5 S (Fig. S10a); similar results were obtained for SARS-CoV M^{pro} (Fig. S10b). For SARS-CoV M^{pro}, a monomer-dimer equilibrium has been found previously by analytical ultracentrifugation *(38)*. Since the peak positions in the c(s) distributions do not change

with protein concentration, the equilibrium is slow on the time scale of sedimentation *(31)*. Therefore, the samples were incubated for ~23 hours at room temperature after dilution before they were subjected to sedimentation analysis.

To determine the dissociation constant (K_d) of the dimerization reaction, binding isotherms for SARS-CoV-2 M^{pro} and SARS-CoV M^{pro} were constructed by calculation of signal-averaged s-values (s_w) by integration of the c(s) distributions in the range where monomers and dimers are observed (Fig. S10c). The binding isotherms, however, cannot be fitted with a monomer-dimer model, since the transitions are too steep and the dimer did not dissociate completely at low concentrations. This may be due to the fact that even after 23 hours of incubation at room temperature, equilibrium was not reached, and to interference with higher oligomers as observed in the c(s) distributions in Figs. S10a and S10b. However, no significant difference between the binding isotherms of SARS-CoV-2 M^{pro} and SARS-CoV M^{pro} could be observed. From the transition range of the binding isotherms, an apparent K_d of about 2.5 µM can be estimated for both proteins.

For the kinetic measurements of enzymatic activity, concentrations of 2.0 µM SARS-CoV-2 M^{pro} were applied. Since these concentrations are in a range where both monomer and dimer are populated and it is known that only the dimer is catalytically active *(9)*, we determined the percentages of dimers at both concentrations. To this end, we subjected triplicates of samples with the respective concentrations directly after dilution to sedimentation velocity analysis and obtained 21% ± 4.2% and 38% ± 5.7% of dimer at 1.0 µM and 2.0 µM, respectively (Fig. S10d). Similar

results, namely 28% ± 8.8% of dimer at 1.0 µM and 42% ± 2.8% at 2 µM, were obtained for SARS-CoV-M^{pro} (Fig. S10e).

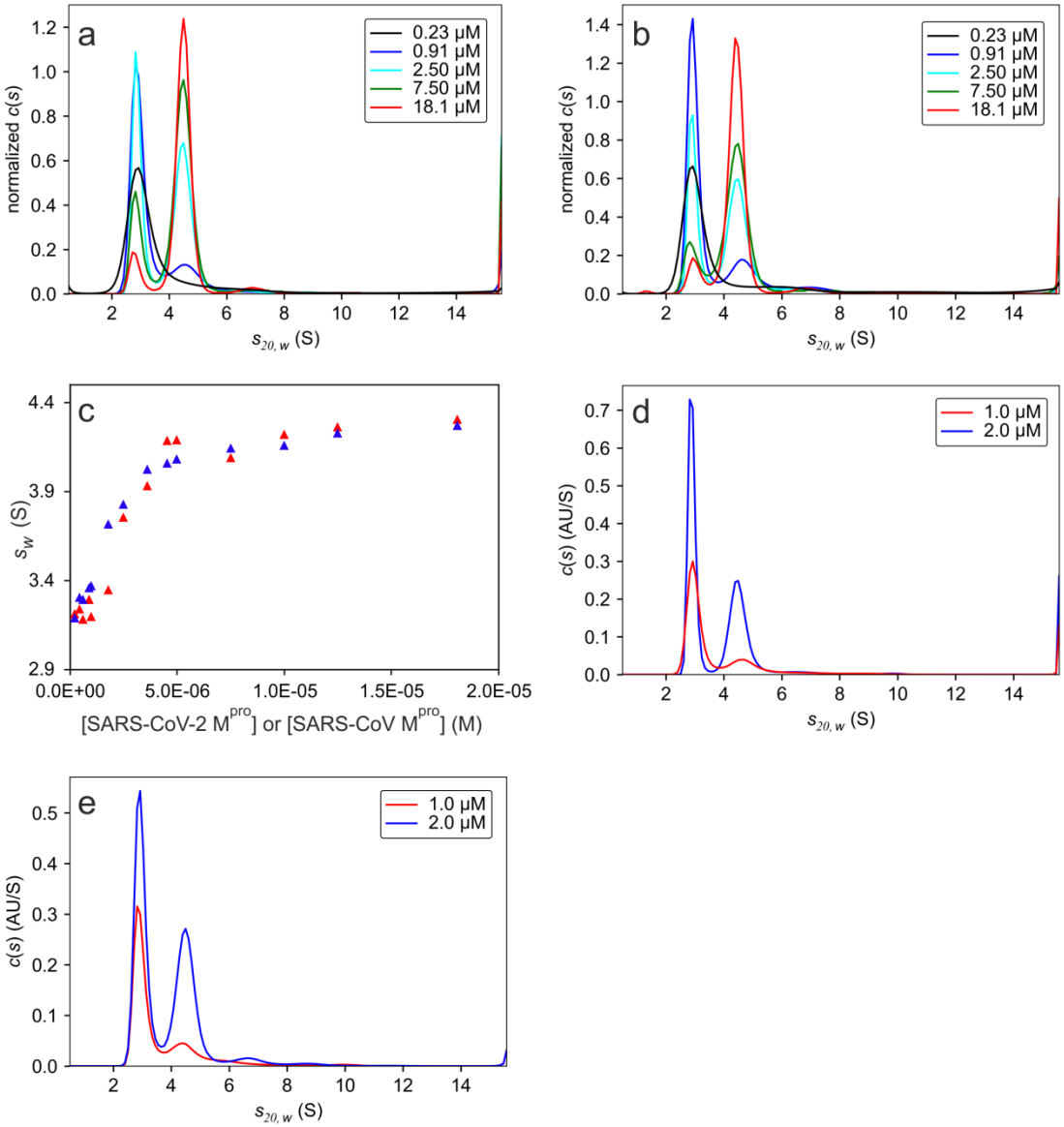

Fig. S10: Sedimentation velocity analysis of the monomer-dimer equilibrium of SARS-CoV-2 M^{pro} and SARS-CoV M^{pro}. Selected c(s) distributions of SARS-CoV-2 M^{pro} **(a)** or SARS-CoV M^{pro} **(b)** measured in a concentration range of 0.23 to 18.1 µM were normalized to the same area for better comparability. It can be clearly seen that equilibrium shifts with increasing protein concentration from almost exclusively monomer ($s_{20,w}$ = 2.9 S) to almost exclusively dimer ($s_{20,w}$ =

4.5 S). As the peak positions do not change with protein concentration, the equilibrium is slow on the time scale of sedimentation *(31)*. Therefore, data were collected after ~23 hours of incubation at room temperature. **(c)** By integration of c(s) distributions such as shown in panels a and b in the range where monomers and dimers were observed, signal-averaged s-values s_w were calculated and plotted as a function of concentration to obtain binding isotherms for SARS-CoV-2 M^{pro} (red) and SARS-CoV M^{pro} (blue). **(d)** In order to determine the percentage of dimers present during kinetic measurements, samples at concentrations of 1.0 µM or 2.0 µM SARS-CoV-2 M^{pro}, respectively, were subjected to sedimentation velocity analysis directly after dilution. Samples were run in triplicates and integration of the c(s) distributions obtained 21% ± 4.2% dimer at 1.0 µM and 38% ± 5.7% at 2 µM. **(e)** Same procedure as in panel **d** but using SARS-CoV M^{pro}, obtained 28% ± 8.8% dimer at 1.0 µM and 42% ± 2.8% at 2 µM. Graphical representation of c(s) distributions, calculation of s_w-values and determination of the percentage of dimers were performed with the program GUSSI *(39)*.

3. Supplementary Tables

Table S2. Diffraction data and model refinement statistics

Protein / Ligand	**M^{pro} free enzyme**	**M^{pro} + 13b (monoclinic form)**	**M^{pro} + 13b (orthorhombic form)**
PDB entry	6Y2E	6Y2F	6Y2G
Data collection statistics			
X-ray source	BESSY 14.2	BESSY 14.2	BESSY 14.2
Wavelength [Å]	0.9184	0.9184	0.9184
V_m [Å^3/Da]	2.01	2.75	2.67
Solvent content [%]	38.8	55.3	54.0
Space group	*C*2	*C*2	$P2_12_12_1$
Unit cell dimensions [Å]	*a* = 114.98, *b* = 53.76, *c* = 44.77	*a* = 98.08, *b* = 80.93, *c* = 51.66	*a* = 68.57, *b* = 101.60, *c* = 103.70
Unit cell dimensions [º]	α = γ = 90, β = 101.24	α = γ = 90, β = 114.84	α = β = γ = 90
Resolution range [a] [Å]	48.53 - 1.75 (1.84 - 1.75)	43.37 - 1.95 (2.06 - 1.95)	41.39 - 2.20 (2.32 - 2.20)
Number of observations	185,991 (27,913)	182,301 (27,374)	492,459 (64,837)
Number of unique reflections	27,173 (3,926)	26,757 (3,919)	37,519 (5356)
Completeness [%]	100.0 (100.0)	100.0 (100.0)	100.0 (100.0)
Mean I/σ(I)	15.0 (2.1)	15.5 (2.2)	13.1 (2.1)
Multiplicity	6.8 (7.1)	6.8 (7.0)	13.1 (12.1)
R_{merge} [b] [%]	0.082 (0.967)	0.076 (0.826)	0.170 (1.388)
R_{pim} [c] [%]	0.034 (0.387)	0.032 (0.335)	0.048 (0.414)
$CC_{1/2}$ [d]	0.999 (0.747)	0.999 (0.809)	0.998 (0.662)
Wilson *B*-factor [Å^2]	23	31	35
Refinement statistics			
Number of unique reflections used for refinement	27,173 (3,926)	26,757 (3,919)	37,519 (5,356)
R_{cryst} [e] /R_{free} [f] [%]	17.12/22.24	17.79/21.91	18.62/24.73
r.m.s.d. in bond lengths [Å]	0.009	0.010	0.010

r.m.s.d. in bond angles [°]	1.6	1.7	1.8
Clashscore [g]	2	3	4
Average B-factor for protein atoms [Å^2]	27	39	44
Average B-factor for ligand atoms [Å^2]	N/A	47	49
Average B-factor for water molecules [Å^2]	37	47	44
Number of protein atoms	2373	2342	4675
Number of ligand atoms	N/A	43	86
Number of water molecules	313	177	313
Ramachandran plot			
Preferred regions [%]	96.37	94.32	93.83
Allowed regions [%]	3.30	5.35	6.17
Outlier regions [%]	0.33	0.33	0

[a] The highest resolution shell is shown in parantheses.

[b] $R_{merge} = \sum_{hkl} \sum_{i=1}^{n} |I_i(hkl) - \bar{I}(hkl)| / \sum_{hkl} \sum_{i=1}^{n} I_i(hkl)$

[c] $R_{pim} = \sum_{hkl} \sqrt{1/(n-1)} \sum_{i=1}^{n} |I_i(hkl) - \bar{I}(hkl)| / \sum_{hkl} \sum_{i=1}^{n} I_i(hkl)$ *(40)*

[d] $CC_{1/2}$ is the correlation coefficient determined by two random half data sets *(41)*

[e] $R_{cryst} = \sum_{hkl} |F_o(hkl) - F_c(hkl)| / \sum_{hkl} |F_o(hkl)|$

[f] R_{free} was calculated for a test set of reflections (5%) omitted from the refinement.

[g] Clashscore is defined as the number of clashes calculated for the model per 1000 atoms (including hydrogens) of the model. Hydrogens were added by MolProbity *(42)*

Table S3. Pharmacokinetic parameters of 13a and 13b after subcutaneous administration (20 mg/kg and 3 mg/kg, resp.)

	13a 20 mg/kg sc	**13b 3 mg/kg sc**
$t_{1/2}$ [h]	1.0 ± 0.1	1.8 ± 0.5
T_{max} [h]	0.4 ± 0.1	0.7 ± 0.3
C_{max} [ng/mL]	334.5 ± 109.2	126.2 ± 31.0
AUC_{0-t} [ng/mL*h]	551.2 ± 67.7	306.6 ± 80.4
MRT [h]	1.6 ± 0.2	2.7 ± 0.8
V_z/F [L/kg]	48.6 ± 7.7	20.4 ± 5.4
Cl/F [mL/kg/min]	565.6 ± 61.0	131.6 ± 26.0

$t_{1/2}$: half-life, T_{max}: time point at which maximal concentration is reached, C_{max}: maximal concentration, AUC_{0-t}: area under the cure from time point 0 until t, MRT: mean residence time, V_z: volume of distribution, Cl: clearance, F: fraction/bioavailability

References

1. P. Zhou, X.-L. Yang, X.-G. Wang, B. Hu, L. Zhang, W. Zhang, H.-R. Si, Y. Zhu, B. Li, C.-L. Huang, H.-D. Chen, J. Chen, Y. Luo, H. Guo, R.-D. Jiang, M.-Q. Liu, Y. Chen, X.-R. Shen, X. Wang, X.-S. Zheng, K. Zhao, Q.-J. Chen, F. Deng, L.-L. Liu, B. Yan, F.-X. Zhan, Y.-Y. Wang, G.-F. Xiao, Z.-L. Shi, A pneumonia outbreak associated with a new coronavirus of probable bat origin. *Nature* **579**, 270–273 (2020). doi:10.1038/s41586-020-2012-7 Medline

2. F. Wu, S. Zhao, B. Yu, Y.-M. Chen, W. Wang, Z.-G. Song, Y. Hu, Z.-W. Tao, J.-H. Tian, Y.-Y. Pei, M.-L. Yuan, Y.-L. Zhang, F.-H. Dai, Y. Liu, Q.-M. Wang, J.-J. Zheng, L. Xu, E. C. Holmes, Y.-Z. Zhang, A new coronavirus associated with human respiratory disease in China. *Nature* **579**, 265–269 (2020). doi:10.1038/s41586-020-2008-3 Medline

3. A. E. Gorbalenya, S. C. Baker, R. S. Baric, R. J. de Groot, C. Drosten, A. A. Gulyaeva, B. L. Haagmans, C. Lauber, A. M. Leontovich, B. W. Neuman, D. Penzar, S. Perlman, L. L. M. Poon, D. Samborskiy, I. A. Sidorov, I. Sola, J. Ziebuhr, Severe acute respiratory syndrome-related coronavirus: The species and its viruses – a statement of the Coronavirus Study Group. *Nat. Microbiol.* (2020). 10.1038/s41564-020-0695-z

4. K. Anand, J. Ziebuhr, P. Wadhwani, J. R. Mesters, R. Hilgenfeld, Coronavirus main proteinase ($3CL^{pro}$) structure: Basis for design of anti-SARS drugs. *Science* **300**, 1763–1767 (2003). doi:10.1126/science.1085658 Medline

5. R. Hilgenfeld, From SARS to MERS: Crystallographic studies on coronaviral proteases enable antiviral drug design. *FEBS J.* **281**, 4085–4096 (2014). doi:10.1111/febs.12936 Medline

6. L. Zhang, D. Lin, Y. Kusov, Y. Nian, Q. Ma, J. Wang, A. von Brunn, P. Leyssen, K. Lanko, J. Neyts, A. de Wilde, E. J. Snijder, H. Liu, R. Hilgenfeld, α-Ketoamides as broad-spectrum inhibitors of coronavirus and enterovirus replication: Structure-based design, synthesis, and activity assessment. *J. Med. Chem.* acs.jmedchem.9b01828 (2020). doi:10.1021/acs.jmedchem.9b01828 Medline

7. J. Tan, K. H. G. Verschueren, K. Anand, J. Shen, M. Yang, Y. Xu, Z. Rao, J. Bigalke, B. Heisen, J. R. Mesters, K. Chen, X. Shen, H. Jiang, R. Hilgenfeld, pH-dependent conformational flexibility of the SARS-CoV main proteinase (M^{pro}) dimer: Molecular dynamics simulations and multiple X-ray structure analyses. *J. Mol. Biol.* **354**, 25–40 (2005). doi:10.1016/j.jmb.2005.09.012 Medline

8. J. Shi, J. Song, The catalysis of the SARS 3C-like protease is under extensive regulation by its extra domain. *FEBS J.* **273**, 1035–1045 (2006). doi:10.1111/j.1742-4658.2006.05130.x Medline

9. K. Anand, G. J. Palm, J. R. Mesters, S. G. Siddell, J. Ziebuhr, R. Hilgenfeld, Structure of coronavirus main proteinase reveals combination of a chymotrypsin fold with an extra

alpha-helical domain. *EMBO J.* **21**, 3213–3224 (2002). doi:10.1093/emboj/cdf327 Medline

10. L. Lim, J. Shi, Y. Mu, J. Song, Dynamically-driven enhancement of the catalytic machinery of the SARS 3C-like protease by the S284-T285-I286/A mutations on the extra domain. *PLOS ONE* **9**, e101941 (2014). doi:10.1371/journal.pone.0101941 Medline

11. N. A. Kratochwil, W. Huber, F. Müller, M. Kansy, P. R. Gerber, Predicting plasma protein binding of drugs: A new approach. *Biochem. Pharmacol.* **64**, 1355–1374 (2002). doi:10.1016/S0006-2952(02)01074-2 Medline

12. H. Yang, M. Yang, Y. Ding, Y. Liu, Z. Lou, Z. Zhou, L. Sun, L. Mo, S. Ye, H. Pang, G. F. Gao, K. Anand, M. Bartlam, R. Hilgenfeld, Z. Rao, The crystal structures of severe acute respiratory syndrome virus main protease and its complex with an inhibitor. *Proc. Natl. Acad. Sci. U.S.A.* **100**, 13190–13195 (2003). doi:10.1073/pnas.1835675100 Medline

13. H. Chen, P. Wei, C. Huang, L. Tan, Y. Liu, L. Lai, Only one protomer is active in the dimer of SARS 3C-like proteinase. *J. Biol. Chem.* **281**, 13894–13898 (2006). doi:10.1074/jbc.M510745200 Medline

14. L. Zhu, S. George, M. F. Schmidt, S. I. Al-Gharabli, J. Rademann, R. Hilgenfeld, Peptide aldehyde inhibitors challenge the substrate specificity of the SARS-coronavirus main protease. *Antiviral Res.* **92**, 204–212 (2011). doi:10.1016/j.antiviral.2011.08.001 Medline

15. J. Tan, S. George, Y. Kusov, M. Perbandt, S. Anemüller, J. R. Mesters, H. Norder, B. Coutard, C. Lacroix, P. Leyssen, J. Neyts, R. Hilgenfeld, 3C protease of enterovirus 68: Structure-based design of Michael acceptor inhibitors and their broad-spectrum antiviral effects against picornaviruses. *J. Virol.* **87**, 4339–4351 (2013). doi:10.1128/JVI.01123-12 Medline

16. P. S. Dragovich, R. Zhou, D. J. Skalitzky, S. A. Fuhrman, A. K. Patick, C. E. Ford, J. W. Meador 3rd, S. T. Worland, Solid-phase synthesis of irreversible human rhinovirus 3C protease inhibitors. Part 1: Optimization of tripeptides incorporating N-terminal amides. *Bioorg. Med. Chem.* **7**, 589–598 (1999). doi:10.1016/S0968-0896(99)00005-X Medline

17. L. Zhang, D. Lin, R. Hilgenfeld, Crystal structure of the complex resulting from the reaction between the SARS-CoV main protease and tert-butyl (1-((S)-3-cyclohexyl-1-(((S)-4-(cyclopropylamino)-3,4-dioxo-1-((S)-2-oxopyrrolidin-3-yl)butan-2-yl) amino)-1-oxopropan-2-yl)-2-oxo-1,2-dihydropyridin-3-yl)carbamate, PDB ID 6Y7M (2020). doi:10.2210/pdb6Y7M/pdb

18. L. Zhu, R. Hilgenfeld, Crystal structure of SARS coronavirus main protease complexed with an alpha, beta-unsaturated ethyl ester inhibitor SG85, PDB ID 3TNT (2012). doi:10.2210/pdb3TNT/pdb

19. Y. Kusov, J. Tan, E. Alvarez, L. Enjuanes, R. Hilgenfeld, A G-quadruplex-binding macrodomain within the “SARS-unique domain” is essential for the activity of the

SARS-coronavirus replication-transcription complex. *Virology* **484**, 313–322 (2015). doi:10.1016/j.virol.2015.06.016 Medline

20. X. Xue, H. Yang, W. Shen, Q. Zhao, J. Li, K. Yang, C. Chen, Y. Jin, M. Bartlam, Z. Rao, Production of authentic SARS-CoV M^{pro} with enhanced activity: Application as a novel tag-cleavage endopeptidase for protein overproduction. *J. Mol. Biol.* **366**, 965–975 (2007). doi:10.1016/j.jmb.2006.11.073 Medline

21. U. Mueller, N. Darowski, M. R. Fuchs, R. Förster, M. Hellmig, K. S. Paithankar, S. Pühringer, M. Steffien, G. Zocher, M. S. Weiss, Facilities for macromolecular crystallography at the Helmholtz-Zentrum Berlin. *J. Synchrotron Radiat.* **19**, 442–449 (2012). doi:10.1107/S0909049512006395 Medline

22. M. Krug, M. S. Weiss, U. Heinemann, U. Mueller, XDSAPP: A graphical user interface for the convenient processing of diffraction data using XDS. *J. Appl. Crystallogr.* **45**, 568–572 (2012). doi:10.1107/S0021889812011715

23. P. Evans, Scaling and assessment of data quality. *Acta Crystallogr. D* **62**, 72–82 (2006). doi:10.1107/S0907444905036693 Medline

24. P. R. Evans, An introduction to data reduction: Space-group determination, scaling and intensity statistics. *Acta Crystallogr. D* **67**, 282–292 (2011). doi:10.1107/S090744491003982X Medline

25. M. D. Winn, C. C. Ballard, K. D. Cowtan, E. J. Dodson, P. Emsley, P. R. Evans, R. M. Keegan, E. B. Krissinel, A. G. Leslie, A. McCoy, S. J. McNicholas, G. N. Murshudov, N. S. Pannu, E. A. Potterton, H. R. Powell, R. J. Read, A. Vagin, K. S. Wilson, Overview of the CCP4 suite and current developments. *Acta Crystallogr. D* **67**, 235–242 (2011). doi:10.1107/S0907444910045749 Medline

26. A. Vagin, A. Teplyakov, Molecular replacement with MOLREP. *Acta Crystallogr. D* **66**, 22–25 (2010). doi:10.1107/S0907444909042589 Medline

27. A. A. Lebedev, P. Young, M. N. Isupov, O. V. Moroz, A. A. Vagin, G. N. Murshudov, JLigand: A graphical tool for the CCP4 template-restraint library. *Acta Crystallogr. D* **68**, 431–440 (2012). doi:10.1107/S090744491200251X Medline

28. P. Emsley, B. Lohkamp, W. G. Scott, K. Cowtan, Features and development of Coot. *Acta Crystallogr. D* **66**, 486–501 (2010). doi:10.1107/S0907444910007493 Medline

29. G. N. Murshudov, P. Skubák, A. A. Lebedev, N. S. Pannu, R. A. Steiner, R. A. Nicholls, M. D. Winn, F. Long, A. A. Vagin, REFMAC5 for the refinement of macromolecular crystal structures. *Acta Crystallogr. D* **67**, 355–367 (2011). doi:10.1107/S0907444911001314 Medline

30. Y. Liu, W. Kati, C. M. Chen, R. Tripathi, A. Molla, W. Kohlbrenner, Use of a fluorescence plate reader for measuring kinetic parameters with inner filter effect correction. *Anal. Biochem.* **267**, 331–335 (1999). doi:10.1006/abio.1998.3014 Medline

31. P. H. Brown, A. Balbo, P. Schuck, Characterizing protein-protein interactions by sedimentation velocity analytical ultracentrifugation. *Curr. Protoc. Immunol.* Chapter 18, Unit 18.15 (2008).

32. P. Schuck, Size-distribution analysis of macromolecules by sedimentation velocity ultracentrifugation and lamm equation modeling. *Biophys. J.* **78**, 1606–1619 (2000). doi:10.1016/S0006-3495(00)76713-0 Medline

33. M. T. Laue, B. D. Shah, T. M. Rigdeway, S. L. Pelletier, in *Analytical Ultracentrifugation in Biochemistry and Polymer Science*, S. Harding, A. Rowe, J. Horton, Eds. (Royal Society of Chemistry, 1992), pp. 90–125.

34. E. F. Pettersen, T. D. Goddard, C. C. Huang, G. S. Couch, D. M. Greenblatt, E. C. Meng, T. E. Ferrin, UCSF Chimera—A visualization system for exploratory research and analysis. *J. Comput. Chem.* **25**, 1605–1612 (2004). doi:10.1002/jcc.20084 Medline

35. Q. Tian, N. K. Nayyar, S. Babu, L. Chen, J. Tao, S. Lee, A. Tibbetts, T. Moran, J. Liou, M. Guo, T. P. Kennedy, An efficient synthesis of a key intermediate for the preparation of the rhinovirus protease inhibitor AG7088 via asymmetric dianionic cyanomethylation of N-Boc-L-(+)-glutamic acid dimethyl ester. *Tetrahedron Lett.* **42**, 6807–6809 (2001). doi:10.1016/S0040-4039(01)01416-2

36. V. M. Corman, O. Landt, M. Kaiser, R. Molenkamp, A. Meijer, D. K. W. Chu, T. Bleicker, S. Brünink, J. Schneider, M. L. Schmidt, D. G. J. C. Mulders, B. L. Haagmans, B. van der Veer, S. van den Brink, L. Wijsman, G. Goderski, J. L. Romette, J. Ellis, M. Zambon, M. Peiris, H. Goossens, C. Reusken, M. P. G. Koopmans, C. Drosten, Detection of 2019 novel coronavirus (2019-nCoV) by real-time RT-PCR. *Euro Surveill.* **25**, (2020). doi:10.2807/1560-7917.ES.2020.25.3.2000045 Medline

37. Y. Zhang, M. Huo, J. Zhou, S. Xie, PKSolver: An add-in program for pharmacokinetic and pharmacodynamic data analysis in Microsoft Excel. *Comput. Methods Programs Biomed.* **99**, 306–314 (2010). doi:10.1016/j.cmpb.2010.01.007 Medline

38. W. C. Hsu, H. C. Chang, C. Y. Chou, P. J. Tsai, P. I. Lin, G. G. Chang, Critical assessment of important regions in the subunit association and catalytic action of the severe acute respiratory syndrome coronavirus main protease. *J. Biol. Chem.* **280**, 22741–22748 (2005). doi:10.1074/jbc.M502556200 Medline

39. C. A. Bräutigam, Calculations and publication-quality illustrations for analytical ultracentrifugation data. *Methods Enzymol.* **562**, 109–133 (2015). doi:10.1016/bs.mie.2015.05.001 Medline

40. M. S. Weiss, R. Hilgenfeld, On the use of the merging *R* factor as a quality indicator for X-ray data. *J. Appl. Crystallogr.* **30**, 203–205 (1997). doi:10.1107/S0021889897003907

41. P. A. Karplus, K. Diederichs, Linking crystallographic model and data quality. *Science* **336**, 1030–1033 (2012). doi:10.1126/science.1218231 Medline

42. V. B. Chen, W. B. Arendall 3rd, J. J. Headd, D. A. Keedy, R. M. Immormino, G. J. Kapral, L. W. Murray, J. S. Richardson, D. C. Richardson, *MolProbity*: All-atom structure validation for macromolecular crystallography. *Acta Crystallogr. D* **66**, 12–21 (2010). doi:10.1107/S0907444909042073 Medline